Proceedings of ASME Turbo Expo 2023
Turbomachinery Technical Conference and Exposition
GT2023
June 26-30, 2023, Boston, Massachusetts

GT2023-101562

THE DEVELOPMENT AND USE OF A NATURAL GAS / OXYGEN BURNER RIG FOR ENVIRONMENTAL BARRIER COATING AND CERAMIC MATRIX COMPOSITE TECHNOLOGY MATURATION

Michael J. Presby, Makoto Endo, Dennis S. Fox, Bryan J. Harder, and Kang N. Lee
National Aeronautics and Space Administration
Glenn Research Center
Cleveland, OH

Leland C. Hoffman, and Michael D. Cuy
HX5, LLC.
Cleveland, OH

ABSTRACT

This work outlines the development of a new natural gas/oxygen (NG/O_2) fueled combustion rig located at the NASA Glenn Research Center for high-temperature environmental durability studies of advanced materials and components at atmospheric pressure. The NG/O_2 burner rig can simulate the high-temperature, high-heat flux, and high-velocity thermal environments encountered in gas turbine engines. It also provides the capability to study environmental effects such as water vapor and other foreign contaminants relevant to these applications. The rig is anticipated to bridge the gap between other laboratory methods such as furnaces, jet-fueled burner rigs, high-heat flux lasers, and more expensive engine rig testing. The NG/O_2 rig is expected to have maximum sample temperature capabilities over 3,000°F (1,649°C) and result in higher water vapor content compared to our Mach 0.3 to Mach 1.0 jet-A burner rigs which is important for characterizing current and next-generation environmental barrier coatings. This paper will provide an overview of the development of the NG/O_2 burner rig, initial characterization, and current research and development efforts on environmental barrier coated ceramic matrix composites.

Keywords: Burner rig, environmental durability testing, environmental barrier coatings (EBCs), ceramic matrix composites (CMCs).

1. INTRODUCTION

The Burner Rig Facility located within the Materials Research Laboratory at the National Aeronautics and Space Administration's Glenn Research Center is used for high temperature materials research including oxidation, corrosion, erosion, and impact. Within the facility are six Mach 0.3 to Mach 1.0 capable, computer-controlled, jet-fueled combustors in individual test cells. These burners operate on Jet-A and pre-heated air. A schematic showing a representation of a standard burner rig is presented in Figure 1. These burner rigs are used as an efficient means of subjecting advanced materials for aero applications to the high-temperature, high-velocity, and thermal cycling environment that more closely approximates engine operating conditions. In addition, modifications and/or additions have been implemented in the burner rigs to study other environmental effects such as salt corrosion, foreign object damage, and solid particle erosion [1-5]. One limitation to the current, atmospheric, jet-fueled burner rigs is that the maximum sample temperature that can be achieved during normal operation is approximately 2,500°F (1,371°C). This restricts the ability to test higher temperature capable materials. For example, next generation environmental barrier coatings (EBCs) and ceramic matrix composites (CMCs) are targeted for temperatures >2,700°F (>1,482°C). Another limitation is the lower water vapor content present in the jet-fueled burner rig combustion, approximately 10% H_2O, limits the study of material recession, which is a critical life-limiting mechanism for silicon (Si)-containing materials such as silicon carbide (SiC)-based CMCs.

To combat these limitations, and to bridge the gap between other laboratory methods (furnaces, high-heat flux lasers, etc.) and engine rig testing, a new natural gas/oxygen (NG/O_2) fueled combustion rig was developed for high temperature environmental durability studies at atmospheric pressure. The NG/O_2 rig can simulate the high-temperature, high-heat flux, and high-velocity thermal environments encountered in gas-turbines. The NG/O_2 rig has a maximum surface temperature capability

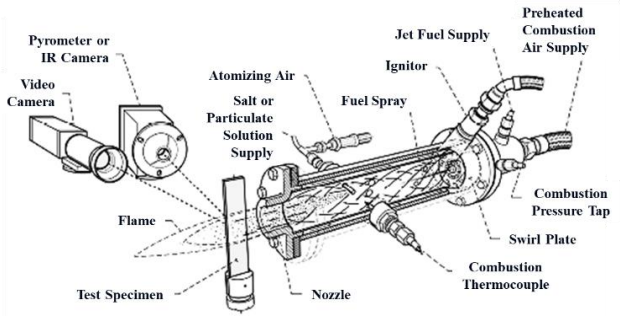

FIGURE 1: Schematic of jet-fueled burner rigs [1].

>3,000°F (>1,649°C) and results in higher water vapor content compared to the jet-fuel atmospheric burner rigs.

This work provides an overview of the development for the new NG/O_2 burner rig, initial characterization, an initial study to characterize the suitability of an EBC/CMC material system for use as a combustion liner for commercial supersonic technology (CST), and a brief synopsis of how the NG/O_2 rig is supporting high temperature EBC/CMC technology maturation under NASA's Hybrid Thermally Efficient Core (HyTEC) project.

2. OVERVIEW OF NATURAL GAS BURNER RIG

2.1 Description

The equipment for the NG/O_2 burner is a custom unit made by Carlisle Machine Works (Millville, NJ) that can consume up to 700 SCFH (standard cubic feet per hour) of natural gas, and 1,500 SCFH of oxygen. A picture of the unit is displayed in Figure 2. An interchangeable selection of 702, 705, or 706 series lathe burner heads can be used to produce flames with different diameters. The 702 series is ¾ inch while the 705 and 707 are 1 inch and 1 ½ inches in diameter, respectively. Figure 3 shows the three different burner heads (nozzles) that can be utilized in the rig. The hoses, solenoid valves, gas regulators, mass flow controllers, controls, check valves, and E-stops are integrated into the power station platform.

The rig has a dual electrode pilot to ignite and sense the flame. If no flame is detected, the system will shut off the natural gas and oxygen flow and alert the operator. A programmable logic controller (PLC) (Allen-Bradley ®) with touchscreen was

FIGURE 2: NG/O_2 burner rig and platform.

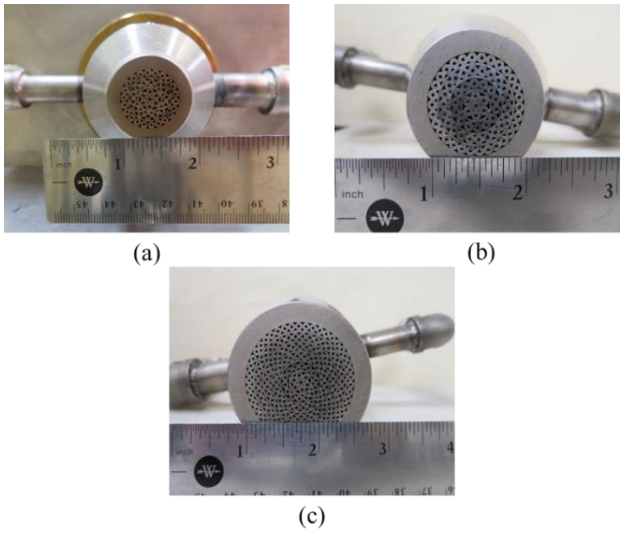

FIGURE 3: Interchangeable lathe burner heads: (a) 702 (¾ inch), (b) 705 (1 inch), and (c) 707 (1 ½ inches).

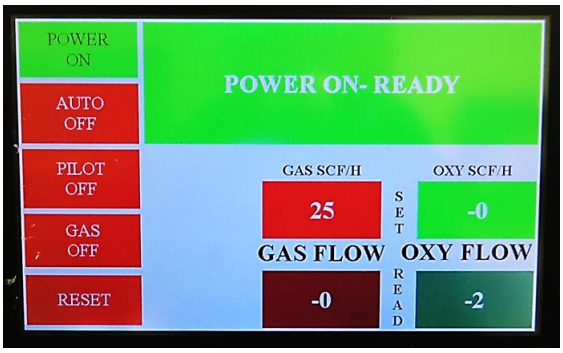

FIGURE 4: Burner programmable logic controller (PLC) touchscreen.

supplied with the burner for operator control and provides ignition, flame-out alarm, safety shutdown, and gas flow control as shown in Figure 4.

The automation software platform Wonderware was used to merge the supplied Allen-Bradley ® PLC with a Modicon PLC to develop one common program for a Human Machine Interface (HMI) screen as shown in Figure 5. The HMI enables additional operator control and monitoring of functions.

The rig is integrated into the building natural gas supply for a continuous flow of fuel while the oxygen is supplied using an on-site oxygen generator system (Oxygen Generating Systems International, North Tonawanda, NY). Implementing an oxygen generator system to provide an uninterrupted supply of oxygen enables continuous (24/7) operation for long-term durability studies.

The oxygen generating system supplies ~93% purity oxygen to the rig. The process of generating oxygen enriched air (~93% O_2 and ~7% N_2) begins by passing filtered, 110-psig shop air from the building supply through a refrigerated air dryer (Parker

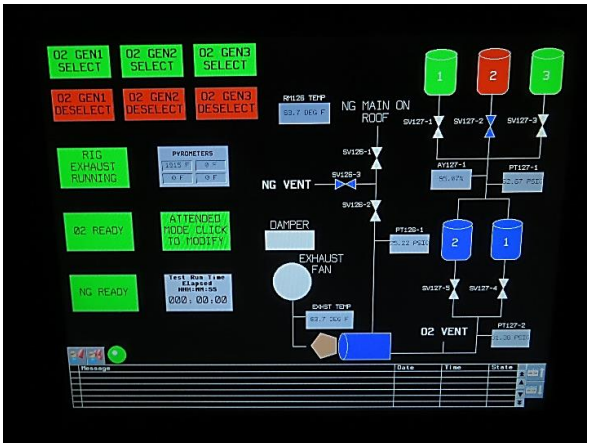

FIGURE 5: Human machine interface (HMI) control screen.

Hannifin, Lancaster, NY) to remove water vapor. The dried air is transferred into a 120-gallon capacity service air holding tank prior to being fed into the oxygen generators. Three OG-500 oxygen generators are used to separate oxygen from the dried shop air using OGSI's Pressure Swing Adsorption (PSA) Technology which centers around a Zeolite molecular sieve [6]. The oxygen enriched air is then stored in two 400 gallon capacity holding tanks that are piped directly to the rig. Figure 6 shows the main components of the oxygen generating system: air dryer, oxygen generators, service air holding tank, and the oxygen enriched air (~93% O_2 and ~7% N_2) holding tanks.

Wonderware Historian is used for data acquisition, data storage, and monitoring the status of the rig. All controls, functions, alerts/alarms, and test specific data (pyrometers, etc.) are displayed in real time and stored to the computer for post-processing. The storage of active alerts/alarms is used to notify the operator and aid in troubleshooting in case of a rig shutdown when operating unattended. The HMI also enables the ability to set upper/lower pyrometer (temperature) limits, and a test timer to safely shut down the rig if an operator is not present.

Figure 7 shows the NG/O_2 burner during its initial operation.

2.2 Chemical Equilibrium Analysis

As discussed previously, the NG/O_2 burner rig uses ~93% purity oxygen. Oxygen enriched combustion provides several

(a) (b) (c)

FIGURE 6: Oxygen generating system: (a) air dryer, (b) oxygen generators, and (c) service air holding tank (left), and oxygen enriched air holding tanks (right).

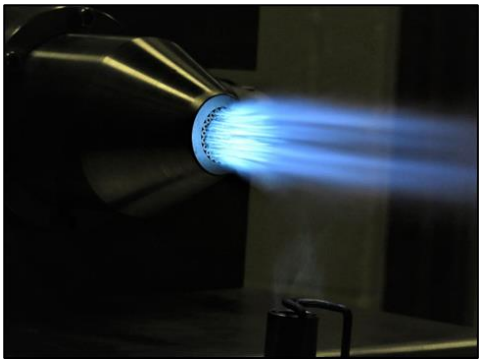

FIGURE 7: NG/O_2 burner rig during initial operation.

benefits over the use of air (21% O_2, 78% N_2, and 1% trace gases) including increased combustion efficiency, lower emissions, and higher combustion temperatures [7]. A basic combustion analysis was performed using the NASA developed Chemical Equilibrium with Applications (CEA) program [8]. The program is used to calculate chemical equilibrium product concentrations and thermodynamic properties for complex mixtures.

The composition of natural gas can vary widely depending upon production region and even supplier. Table 1 shows the values that were used in the initial analysis. These values were obtained from the John Zink Combustion Handbook [9] and were determined to be a reasonable approximation to the range of values that can be found in the Ohio (USA) region. Since methane is the major component of natural gas (>93 vol.%), the CEA analysis was also run using 100 vol.% methane to see if any significant difference in flame temperature and/or gas species concentration is predicted.

TABLE 1. Natural gas composition used for CEA analysis.

Fuel Gas Component	Chemical Formula	Volume %	Weight %
Methane	CH_4	93.4	87.4
Ethane	C_2H_6	2.7	4.7
Propane	C_3H_8	0.6	1.5
Butane	C_4H_{10}	0.2	0.7
Carbon Dioxide	CO_2	0.7	1.8
Nitrogen	N_2	2.4	3.9
Total	---	100.0	100.0

The adiabatic flame temperature as a function of equivalence ratio is shown in Figure 8 for combustion in air, and oxygen enriched air. The calculation was performed with both the fuel and oxidizer at 77°F (298.15 K) and 14.7 psia (1 atm). The benefit of using oxygen enriched air is evident from the higher adiabatic flame temperature. It is also observed that there is no significant difference in the predicted flame temperature for the natural gas composition in Table 1 and 100 vol.% methane.

It is important to recognize that the actual flame temperature will be cooler than the adiabatic flame temperature due to incomplete combustion, heat loss to the surrounding, dilutants entering the flame, etc. Figure 9 shows a first attempt to measure

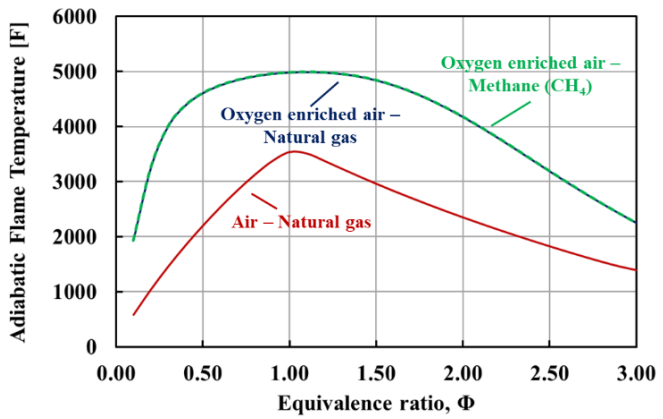

FIGURE 8: Adiabatic flame temperature versus equivalence ratio, Φ, for natural gas combustion with air and oxygen enriched air, and methane combustion with oxygen enriched air. Fuel and oxidizer (air or oxygen enriched air) at 77°F and 14.7 psia.

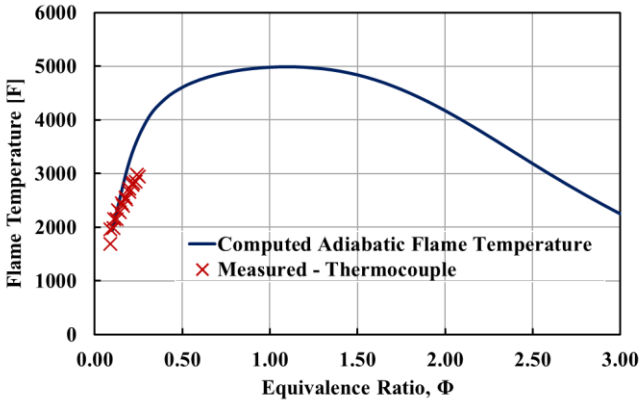

FIGURE 9: Computed adiabatic flame temperature for natural gas and oxygen enriched air, and measured flame temperature at 5.5 inches from the nozzle in the NG/O_2 burner rig using a thermocouple.

the flame temperature using a platinum bead thermocouple placed approximately 5.5 inches from the nozzle. Test articles are typically placed between 5 and 6 inches from the nozzle exit depending upon sample fixturing, orientation, etc. Platinum has a melting temperature of ~3,200°F which limited the ability to obtain thermocouple measurements above an equivalence ratio of ~0.25.

The gas species concentration (mol%) as a function of equivalence ratio, Φ is given in Figure 10. The primary species of interest is H_2O which is calculated to range from ~10 to 40% depending on equivalence ratio. For comparison, the H_2O concentration in the jet-fueled burner rigs is ~10% or less. Similarly, no significant difference in predicted gas species concentration for natural gas and 100 vol.% methane is observed. The results of the equilibrium analysis provide a first insight into the combustion environment over a range of equivalence ratios. However, in application, chemical kinetics is required to

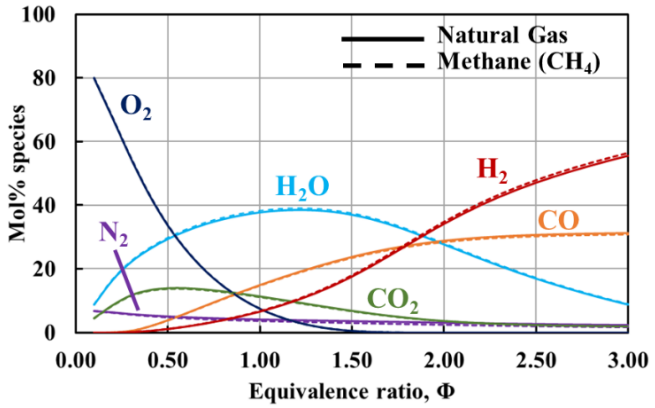

FIGURE 10: Gas species concentration from CEA analysis as a function of equivalence ratio, Φ for natural gas and 100 vol%. methane.

understand the rates of reactions and how the gas species concentration, temperature, and velocity changes with time. This will be briefly introduced and discussed in Section 2.3.

2.3 Combustion Simulations

Chemical equilibrium analysis is valid for the limit of infinitely fast reaction rates, or in other words, it is a thermodynamic limit. In actuality, the combustion process is more complex, and the process is governed by finite rates. To develop a better understanding of the combustion process, simulations are being performed using chemical kinetics mechanisms. For simplicity, and based on the results from CEA, 100 vol.% methane is used to approximate natural gas, and appropriate kinetics mechanisms for methane – oxygen combustion are being investigated and utilized.

OpenNCC (a publicly releasable version of the National Combustion Code [10-12]) and FUN3D (NASA Langley's CFD Solver [13]), are used to perform the simulations. Figure 11 shows one quarter of the 702 (¾ inch) burner nozzle that is modeled with symmetry conditions. All initial experiments in the rig have utilized the ¾ inch nozzle. Future work will be required to investigate the use of the 705 (1 inch) and 707 (1 ½ inches) nozzles.

Figure 12 shows the overall geometry of the computational domain. A region with a high mesh density exits between the

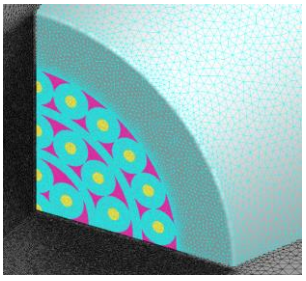

FIGURE 11: Computational mesh of 702 (¾ inch) nozzle exit: fuel port (yellow), nozzle wall (cyan), and oxidizer (pink).

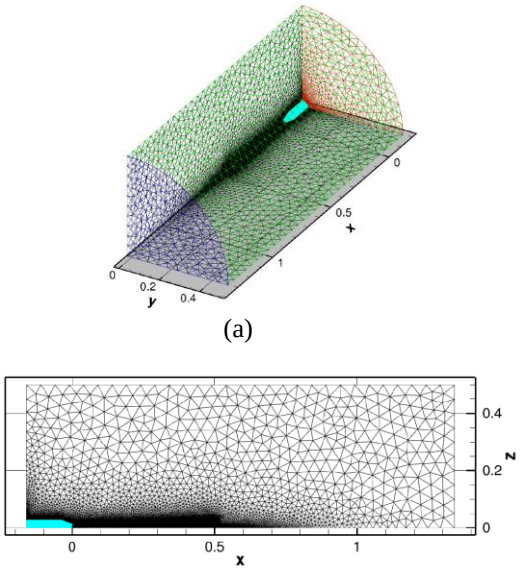

(a) (b)

FIGURE 12: Overall view of the computational domain – total cell count: ~13 million. (a) 3D view: domain inlet (red), domain outlet (blue), domain side (green). (b) 2D view of the symmetry plane.

nozzle exit and approximately 0.5 m from the nozzle exit to capture mixing of the fuel, oxidizer, and surrounding air. Figure 13 displays an example of the information extracted from the simulations showing gas temperature, gas velocity, and H_2O mole fraction as a function of distance from the nozzle exit. Future computational work will focus on incorporating an EBC/CMC sample geometry for conjugate heat transfer studies which will be coupled with experimental efforts.

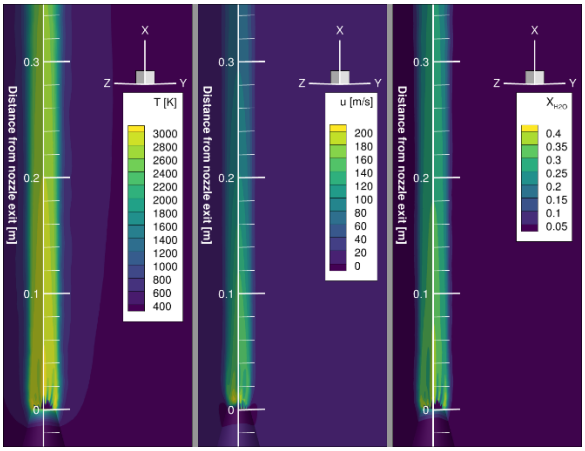

FIGURE 13: Example of information extracted from combustion simulation: gas temperature T[K], gas velocity u[m/s], and H_2O mole fraction X_{H2O}.

2.4 Heat Flux Characterization

An initial measurement of the heat flux in the NG/O_2 burner rig was conducted with a 64-Series Gardon Gauge water-cooled heat flux sensor (MEDTHERM Corporation, Huntsville, AL) as shown in Figure 14 (a). The sensor was positioned normal (90°) to the flame at an initial stand-off distance of 5.5 inches from the nozzle as displayed in Figure 14 (b). Three heat flux curves were generated by holding the oxygen constant at three different flows: 470 (minimum oxygen flow), 600, and 700 SCFH. The natural gas flow was then increased from a starting value of 25 SCFH (the minimum flow used for ignition). The results are shown in Figure 15 (a) for the three oxygen flow rates as a function of natural gas flow, and in Figure 15 (b) as a function of fuel/air (F/A) ratio, and equivalence ratio, Φ.

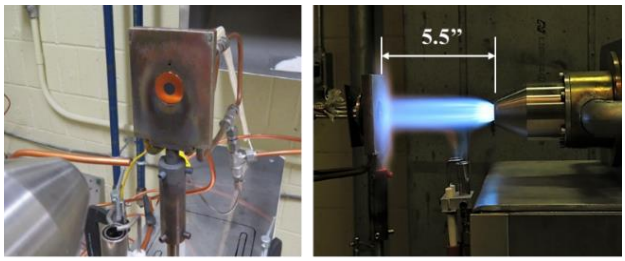

(a) (b)

FIGURE 14: Heat flux measurement in NG/O_2 burner rig: (a) water-cooled Gardon Gauge sensor, and (b) measurement at 5.5 inch nozzle-to-sensor stand-off distance.

The measured heat flux increases with increasing natural gas flow (with constant oxygen flow) until a maximum is reached, and then begins to decrease with a further increase in natural gas flow. When plotted as a function of F/A ratio, or equivalence ratio, Φ, the three curves coincide with one another showing a primary dependence of heat flux on the F/A ratio (or similarly, equivalence ratio, Φ) where the maximum occurs at slightly fuel-rich mixtures, Φ ≈ 1.1. The measured heat flux ranges from ~30 to 210 W/cm^2. For comparison the peak heat flux measured using the same sensor in the jet-fueled burner rigs is ~100 W/cm^2 which highlights the higher heat flux capability of the NG/O_2 burner rig.

It should be noted that care must be taken when interpreting the heat flux results in Figure 15. The Gardon Gauge sensor is actively cooled using water, so the measured values represent a cold-wall heat flux. In addition, the NG/O_2 burner rig environment is mixed mode, consisting of convective and radiative heat transfer. The measurement can be highly sensitive to local convection, and while water-cooled sensors such as the Gardon Gauge can be successfully implemented in mixed mode environments, corrections may be required [14-15]. Nonetheless, these measurements serve as an initial assessment, and provide a relative comparison to the jet-fueled burner rigs.

3. OXIDATION AND RECESSION EXPERIMENT

In the high, water vapor partial pressure environment of a gas turbine engine, Si-containing materials are susceptible to significant surface recession due to the reaction of the protective silica (SiO_2) scale with water vapor to form gaseous $Si(OH)_4$ [16]. This phenomenon is one of the life-limiting mechanisms

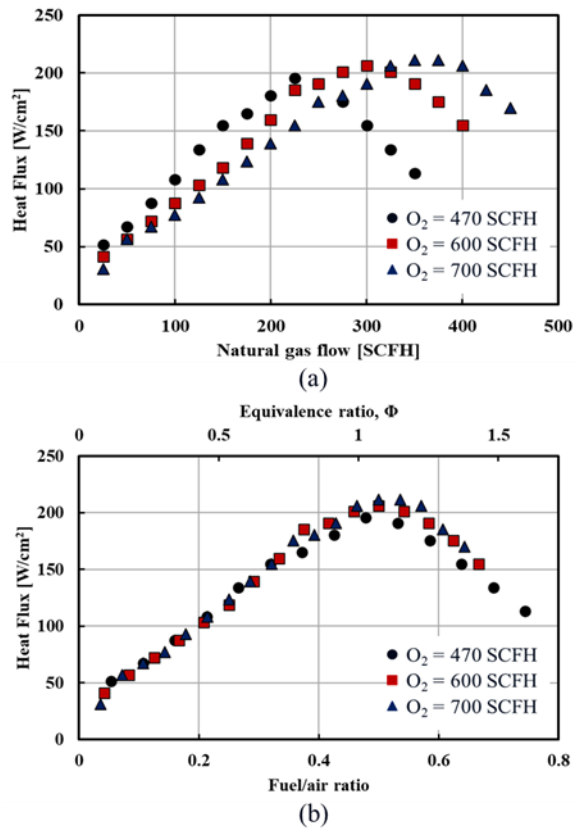

FIGURE 15: Gardon Gauge heat flux measurements for three different oxygen flow rates (470, 600, and 700 SCFH): (a) heat flux as a function of natural gas flow (SCFH), and (b) heat flux as a function of fuel/air, and equivalence ratio, Φ.

for SiC-based materials such as silicon carbide fiber reinforced, silicon carbide matrix (SiC/SiC) CMCs and is controlled via the following reactions:

$$SiC + 1.5O_{2\,(g)} \rightarrow SiO_2 + CO_{(g)} - \text{Oxidation} \quad (1)$$

$$SiC + 3H_2O_{(g)} \rightarrow SiO_2 + CO_{(g)} + 3H_{2\,(g)} - \text{Oxidation} \quad (2)$$

$$SiO_2 + 2H_2O_{(g)} \rightarrow Si(OH)_{4\,(g)} - \text{Recession} \quad (3)$$

To combat this phenomenon, environmental barrier coatings (EBCs) were developed [17].

Due to the importance of understanding material recession, particularly for gas turbine materials such as SiC/SiC CMCs, an initial experiment on monolithic SiC (Hexoloy® SA, Saint - Gobain, Worcester, MA) was performed to assess the capability of the NG/O_2 burner rig for oxidation and recession studies. This initial set of experiments is also used as an initial evaluation to see how the NG/O_2 burner rig compares to other laboratory facilities.

The dimensions of the SiC bars used for the oxidation and recession tests were 152.4 mm (6 inches) by 25.4 mm (1 inches) by 6.35 mm (0.25 inches) (l x w x h). The bars were held in place using a vice-clamp fixture with a nozzle exit to sample distance

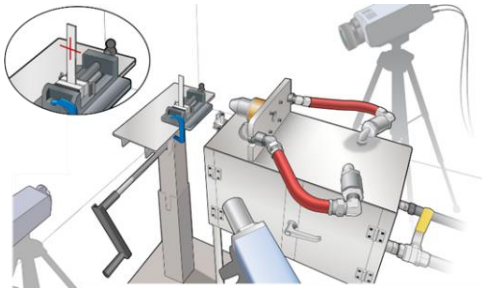

FIGURE 16: Illustration of test set-up for SiC oxidation and recession testing.

of 139.7 mm or 5.5 inches. An illustration of the test set-up is shown in Figure 16. Five samples were tested at the leading edge (LE) temperatures and equivalence ratios listed in Table 2. Note that one sample, sample 2, was pre-oxidized prior to testing in the rig. Since the stand-off distance was kept constant for every sample, different temperatures were achieved by adjusting the equivalence ratio, Φ. The LE temperature was measured using a Williamson Corporation (Concord, MA) ratio pyrometer. A second ratio pyrometer was aimed at the intersection of the midplane of the sample width and the midplane of the flame as denoted by the crosshairs in the inset of Figure 16. A FLIR A6798sc thermal imaging camera was used to understand the thermal gradients within the sample during testing.

All samples were tested using the 702 (¾ inch) nozzle and an example of a SiC bar during a test is shown in Figure 17. The specific weight change for the five SiC samples are shown in Figure 18 and the linear volatilization rates are given in Table 3. The specific weight change was calculated using a hot zone equivalent to the nozzle diameter (1.905 cm or ¾ inch). Material recession is assumed to primarily occur within this region of high velocity combustion gases; however, there is some expansion of the flame after the nozzle. The effect of this expansion will need to be further understood using the coupled experimental and computational efforts.

TABLE 2. Test matrix for SiC oxidation-recession.

Sample	Leading-Edge Temperature [°F/(°C)]	Φ
1	2,400 (1,316)	0.38
2	2,400 - pre-oxidized (1,316)	0.38
3	2,700 (1,482)	0.52
4	2,900 (1,593)	0.62
5	3,000 (1,649)	0.75

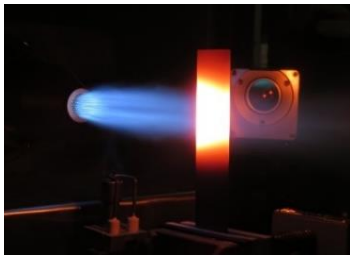

FIGURE 17: SiC bar during oxidation-recession testing at 2,700°F LE temperature.

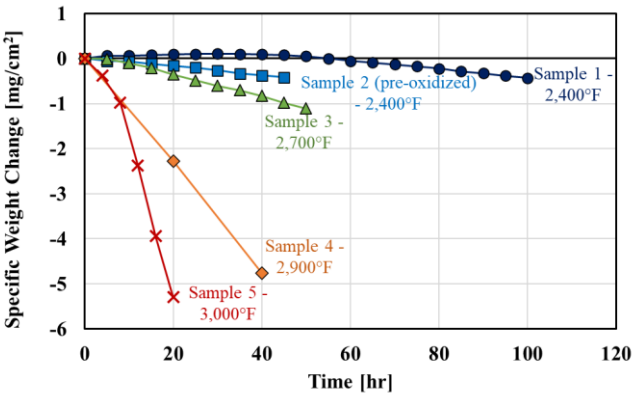

FIGURE 18: Specific weight change of SiC samples at the LE temperatures listed in Table 2.

Figure 19 shows a comparison of the linear volatilization rates obtained for SiC in the NG/O_2 rig to those obtained in other laboratory scale facilities: thermogravimetric analysis (TGA) [18-19], jet-fueled burner rig (Mach 0.3) [20], and high-pressure burner rig (HPBR) [21]. Due to the presence of thermal gradients, and the fact that linear volatilization is temperature dependent, an average temperature of the sample within the flame region (1.905 cm x 2.54 cm) was determined using the IR thermal imaging. As such, two curves are shown for the NG/O_2 rig data where the linear volatilization rates are plotted as a function of LE temperature, and the average temperature in the flame region.

TABLE 3. Linear volatilization (recession) rates for the samples tested under the conditions shown in Table 2. The volatilization rates were calculated based on a 1.907 cm (¾ inch) hot zone.

Sample No.	Linear Volatilization Rates [mg/(cm^2 hr)]
1	0.0103
2	0.0107
3	0.0252
4	0.1190
5	0.3627

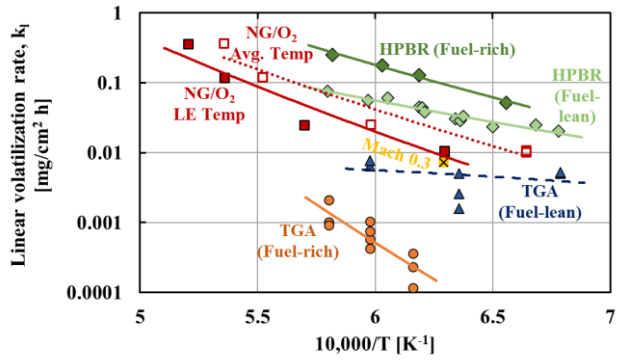

FIGURE 19: Linear volatilization rate of SiC bars tested in NG/O_2 burner rig as compared to results from other studies: TGA [18-19], Mach 0.3 [20], and HPBR [21].

In general, the average temperature was approximately 100 to 150°F lower than the LE temperature. Based on Figure 19, it is observed that the overall volatilization rates obtained in the NG/O_2 rig lie somewhere between those obtained in the atmospheric Mach 0.3 burner rig and the HPBR. This highlights that the NG/O_2 rig can be a reasonable screening tool for understanding recession in a laboratory combustion environment prior to testing in more expensive engine rig tests. The SiC oxidation-recession tests also serve as a calibration or baseline data set toward understanding the performance of the rig.

Ideally, the linear volatilization rates between different studies and facilities should be compared on the basis of the flux of volatile species, $Si(OH)_4$. For $Si(OH)_4$, the flux, k_l, is proportional to sample temperature, T, gas velocity, v, partial pressure of H_2O, $P(H_2O)$, and total pressure, P_t as follows

$$k_l \propto e^{-Q/RT} \frac{v^{1/2} P(H_2O)^2}{P_t^{1/2}} \quad (4)$$

where Q is the activation energy, and R is the universal gas constant [21]. Future work will couple the experimental oxidation-recession results with the combustion analysis and simulations to better understand the volatilization rate based on the temperature, gas velocity, and partial pressure of H_2O. Additional computational methods should also be explored in the future to better understand how oxidation and recession will vary in the presence of a thermal gradient, but this initial analysis is expected to give a first approximation of the SiC oxidation-recession in the NG/O_2 rig.

4. COMMERCIAL SUPERSONIC TECHNOLOGY (CST): EBC/CMC COMBUSTOR LINER

The CST project at NASA is looking to develop tools, technologies, and knowledge that will help overcome the technical barriers to practical commercial supersonic flight such as sonic boom, fuel efficiency, high-altitude emissions, and airport community noise [22]. EBC/CMC technology has the potential to aid supersonic transport through increased fuel efficiency and high-altitude emission reduction due to their low density (~⅓ the density of Ni-based superalloys), and high temperature capability that can lead to reduced cooling requirements. Recent work on the emissions at high power conditions applicable to supersonic cruise showed that changes to the fraction of combustor air required for liner cooling significantly affect NOx emissions [23]. Air used to cool the combustor liner is not available to mix with the fuel which leads to increased flame zone fuel-air ratio that leads to increased NOx emissions. As such, the ability to reduce liner cooling due to the use of higher temperature capable materials such as EBCs and CMCs will result in reduced emissions.

Under the CST project, EBC/CMC systems are being investigated to understand the upper use temperature of the system without cooling air, with back side cooling, and effusive cooling techniques. Preliminary work in the uncooled configuration has been performed on a melt-infiltrated (MI) SiC/SiC CMC. The MI SiC/SiC CMC is protected by an EBC

consisting of a silicon (Si) bond coat and a ytterbium disilicate ($Yb_2Si_2O_7$) topcoat. A 3 inch by 3 inch sample was tested in the NG/O_2 rig at an EBC surface temperature of 2,700°F (1,482°C). An illustration of the test set-up is shown in Figure 20. The overall test set-up for the 3 inch x 3 inch panel was similar to the SiC oxidation-recession testing but utilizes a different sample fixture. Based on knowledge of the thermal conductivity of the system, it was estimated that the thermal gradient through the $Yb_2Si_2O_7$ topcoat and Si bond coat was approximately 300°F leading to a CMC interface temperature of 2,400°F which is the upper use temperature of the MI CMC.

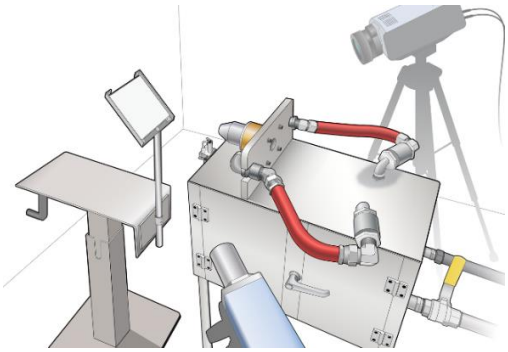

FIGURE 20: Test set-up for 3 inch by 3 inch EBC/CMC samples.

Two EBC/CMC samples were tested: (1) to 25 hours, and (2) to 250 hours with periodic shutdowns for nozzle cleaning and rig inspections. The samples were then destructively evaluated to characterize the thermally grown oxide (TGO) thickness since TGO growth will be life-limiting to the EBC system [24-25]. It is worth noting that the initial purpose of this study is to look at the temperature capability and durability of the EBC/CMC under relevant combustion conditions. Future work will be required to focus on thermo-mechanical aspects.

Figure 21 shows polished cross-sections of the 25 hour and 250 hour samples taken at the center of the sample in the hot – zone. The average TGO thickness for the 25 hour sample was 1.3 µm and the average TGO thickness for the 250 hour sample was 4.3 µm. This corresponds to a parabolic oxidation growth rate, k_p of 0.074 µm^2/hr. Qualitative assessments of this EBC show that the critical TGO thickness resulting in spallation is somewhere between 20 and 30 µm. Assuming 20 µm as the limit, the life of the EBC due to oxidation would be reached after approximately 5,400 hours under these conditions: 2,700°F (1,482°C) EBC surface, 2,400°F (1,316°C) CMC interface temperature, with no backside cooling (free convection). It must be noted that the synergy between other environmental/failure mechanisms can result in shorter lifetime.

In the 250 hour sample, a crack initiated through the EBC as shown in Figure 22. Based on IR thermal imaging, the crack initiated approximately 18 hours into the test and propagated down to the Si bond coat – CMC substrate interface. The crack was located slightly above the center of the sample but still within the hot zone. The difference in TGO thickness under the

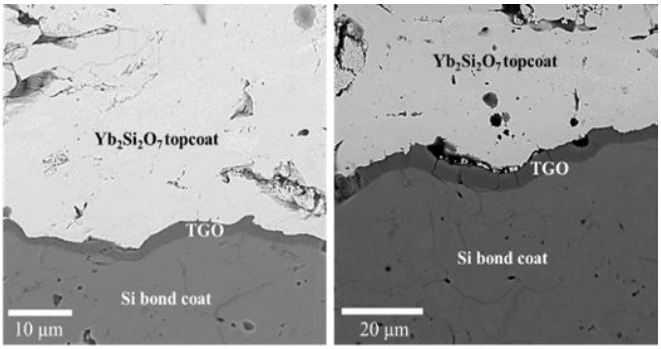

(a) (b)

FIGURE 21: Polished cross-sections of (a) 25-hour sample and (b) 250-hour sample showing TGO thickness. Note difference in scale between the two images.

EBC and within the crack is evident. The average TGO thickness on the exposed CMC substrate in the cracked region was 8.8 µm which was approximately twice the thickness of the TGO under the EBC in an uncracked region of the sample. This highlights the reduction of the TGO growth rate under the EBC and shows the importance of maintaining the integrity of the EBC as defects such as cracks can lead to deleterious effects.

Investigations on NASA-developed modified $Yb_2Si_2O_7$-based EBCs to improve oxidation life are underway [25]. Previous work showed that modified $Yb_2Si_2O_7$-based EBCs tested under steam cycling, 90% H_2O / 10% O_2 at 2,400°F (1,316°C) showed approximately 20x improvement in oxidation life compared to the baseline $Yb_2Si_2O_7$ EBC [25]. Slowing the TGO will be critical for the durability and life requirements for commercial supersonic transport.

5. HYBRID THERMALLY EFFICIENT CORE (HYTEC): ENHANCED COMBUSTOR MATERIALS AND HIGH TEMPERATURE TURBINE MATERIALS

The HyTEC project aims to develop small core turbofan engine technologies to enable fuel burn reductions, additional use of electric airplane systems through power extraction, and to advance engine operability and compatibility with sustainable aviation fuels [26]. Technology advancement under NASA's HyTEC project will provide environmental and cost benefits for the next generation of single-aisle class aircraft. The technology portfolio for HyTEC includes High Pressure Compressor, Enhanced Combustor Materials, High-Temperature Turbine Materials, Advanced High Pressure Turbine Aerodynamics, and Turbofan Power Extraction [26]. Within the materials portfolio, CMC combustor liners are being developed to increase performance and durability, and to reduce cooling and emissions. In addition, CMCs and EBCs capable of withstanding higher temperatures, up to 2,700°F (1,482°C) CMC and 3,000°F (1,649°C) EBC are being developed for turbine blades and vanes. In Phase I of the HyTEC project, CMC and EBC technology will be tested in laboratory-relevant environments and advanced to a technology readiness level (TRL) of 4 or 5, and then further advanced to TRL 6 in Phase II through integration of the technologies in an engine core demonstrator.

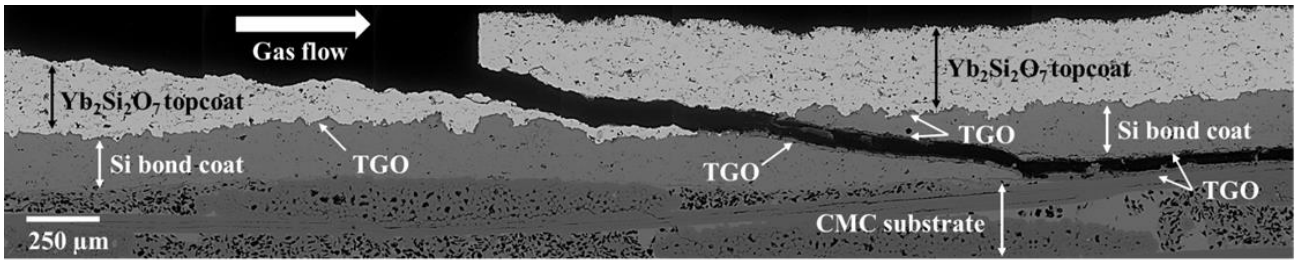

FIGURE 22: Polished cross-section of the 250 hour sample showing the crack that propagated through the $Yb_2Si_2O_7$ topcoat, Si bond coat, and along the Si bond coat – CMC interface. The direction of gas flow is also noted.

The NG/O_2 burner rig is being utilized for the high temperature EBC/CMC development with a target EBC surface temperature of 3,000°F (1,649°C) and an EBC/CMC interface temperature of 2,700°F (1,482°C). The interface temperature is controlled by adjusting the backside cooling air flow rate and fuel/air ratio to achieve the desired thermal gradient. NASA oxide-based high temperature EBCs have been developed to enable temperatures above the melting point of the Si bond coat (1,414°C) used in the baseline and modified $Yb_2Si_2O_7$-based EBCs [27]. The high temperature EBCs have been demonstrated to a TRL of 3 using steam cycling and laser thermal gradient testing. Technology advancement to TRL 4 is achievable through successful testing in the NG/O_2 combustion environment. Several high-temperature capable EBC architectures are being investigated within the HyTEC project. An example of the NASA-developed high temperature EBC during a test in the NG/O_2 rig is shown in Figure 23. These tests are being performed on 3 inch by 1 inch samples with two spacers for insulation to minimize lateral heat loss with the flame impinging on the center of the sample. The target duration of a given test is 250 hours. Tests are run continuously with periodic shutdowns to clean the nozzle of carbon build-up and rig inspections. Successful architectures that survive the 250 hours in the NG/O_2 burner rig will be further developed and tested in a newly designed materials test section in NASA's CE-5 Combustor Test Stand to achieve TRL 5. The CE-5 test stand will expose the developed EBC/CMC technology to relevant temperatures (3,000°F / 1,649°C) and pressures (up to 400psig / ~27 atm) that can be observed in gas-turbine environments.

Figure 24 shows the newly designed materials test section for the CE-5 test stand. The new test section is modular and has

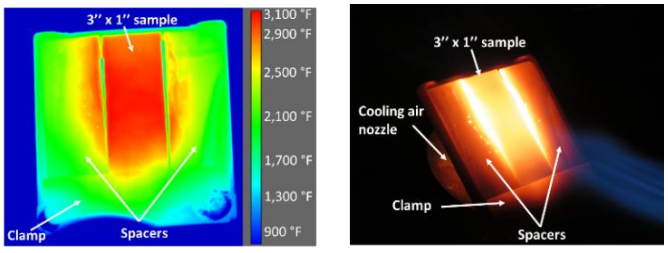

(a) (b)

FIGURE 23: NASA-developed high temperature EBC testing of a 3 inch x 1 inch sample in the NG/O_2 burner rig (a) IR thermal image and (b) optical image.

dimensions of 3.5 inches in width, 3.5 inches in height, and 5.8 inches in length. The test section can accommodate a wide range of samples from flat plates to more complex airfoil geometries. The samples can be actively cooled, and various ports have been integrated for instrumentation such as thermocouples, pyrometers, and IR thermal imaging cameras.

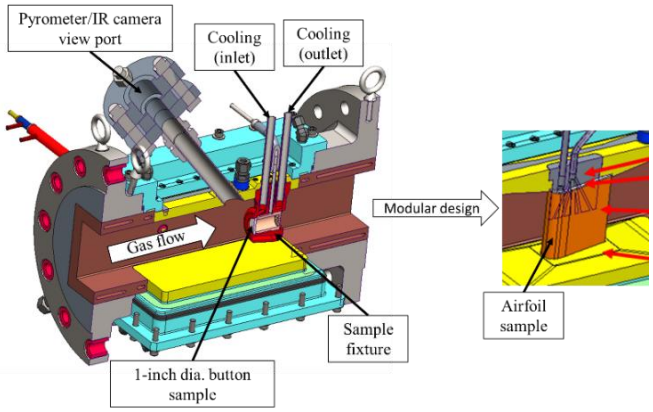

FIGURE 24: Newly developed materials test section for NASA's CE-5 combustion facility. Modular design enables flexibility in sample architecture/geometry and instrumentation.

6. CONCLUSIONS

A new atmospheric burner rig facility using natural gas and 93% oxygen was developed to test and characterize current and next generation gas-turbine materials. The facility is cost-effective and is an efficient means of screening advanced materials in a high temperature combustion environment. The facility was designed to run short term screening tests, and long-term durability tests with the ability to run continuously (24/7). Coupled experimental and computational analyses are utilized to characterize and develop a fundamental understanding of the rig. The rig also bridges a gap between other laboratory methods such as: furnaces, high-heat flux lasers, atmospheric jet-fueled burner rigs, and more expensive engine rig testing. The NG/O_2 burner rig is currently utilized by NASA's Aeronautics Research Mission Directorate (ARMD) projects to mature EBC/CMC technology with a focus on next generation, high temperature EBC (3,000°F / 1,649°C) and CMC (2,700°F / 1,482°C) development.

ACKNOWLEDGEMENTS

This work was supported by the Aeronautics Research Mission Directorate (ARMD) Hybrid Thermally Efficient Core (HyTEC) Project, Commercial Supersonic Technology (CST) Project, and Transformational Tools and Technologies (TTT) Project.

REFERENCES

[1] Fox, D. S., Miller, R. A., Zhu, D., Perez, M., Cuy, M. D., and Robinson, R. C., "Mach 0.3 Burner Rig Facility at the NASA Glenn Materials Research Laboratory," *NASA/TM – 2011-216986*, 2011, https://ntrs.nasa.gov.

[2] Santoro, G. J., Gokoglu, S. A., Kohl, F. J., Stearns, C. A., Rosner, D. A., "Deposition of Na_2SO_4 from Salt-Seeded Combustion Gases of a High Velocity Burner Rig," *NASA/TM – 83751*, 1984, httpntrs.nasa.gov.

[3] Bhatt, R. T., Choi, S. R., Cosgriff, L. M., Fox, D. S., and Lee, K. N., "Impact Resistance of Environmental Barrier Coated SiC/SiC Composites," *Materials Science and Engineering: A*, vol. 476, no. 1-2, pp. 8-19, 2008.

[4] Smialek, J. L., Cuy, M. D., Harder, B. J., Garg, A., and Rogers, R. B., "Durability of YSZ Coated Ti_2AlC in 1300°C High Velocity Burner Rig Tests," *Journal of the American Ceramic Society*, vol. 103, no. 12, pp. 7014-7030, 2020.

[5] Presby, M. J., and Harder, B. J., "Solid Particle Erosion of a Plasma Spray – Physical Vapor Deposition Environmental Barrier Coating in a Combustion Environment," *Ceramics International*, vol. 47, no. 17, pp. 24403-24411, 2021.

[6] "What is Pressure Swing Adsorption Technology," *Oxygen Generating Systems Intl.*, https://www.ogsi.com/pressure-swing-adsorption-technology.

[7] Hendershot, R. J., Lebrecht, T. D., and Easterbrook, N. C., "Use Oxygen to Improve Combustion and Oxidation," *Chemical Engineering Progress*, 2010.

[8] McBride, B. J., and Sanford, G., "Computer Program for Calculation of Complex Chemical Equilibrium Compositions and Applications II. User's Manual and Program Description," *NASA Reference Publication*, 1996, https://ntrs.nasa.gov.

[9] Baukal, C. E., and Schwartz, R. E., "The John Zink Combustion Handbook," Boca Raton, FL, *CRC Press LLC*, 2001.

[10] Endo, M., Tacina, K., Hicks, Y., Capil, T., and Moder, J., "Numerical Simulation of Lean Blowout of Alternative Fuels in 7-element Lean Direct Injector," *AIAA Propulsion and Energy 2021 Forum*, 2021.

[11] Chen, K. H., Torris, A. T., Quealy, A., and Liu, N. S., "Benchmark Test Cases for the National Combustion Code," *34th AIAA/ASME/SAE/ASEE Joint Propulsion Conference and Exhibit*, 1998.

[12] Shih, T. H., Chen, K. H., and Liu, N. S., "A Non-Linear *k*-ε Model for Turbulent Shear Flows," *34th AIAA/ASME/SAE/ASEE Joint Propulsion Conference and Exhibit*, 1998.

[13] Biedron, R. T., et. al., "FUN3D Manual: 13.7" https://fun3d.larc.nasa.gov/papers/FUN3D_Manual-13.7_CORRECTED_COPY.pdf.

[14] Pullins, C. A., and Diller, T. E., "Direct Measurement of Hot-Wall Heat Flux," *Journal of Thermophysics and Heat Transfer*, vol. 26, no. 3, pp. 430-438, 2012.

[15] Lam, C. S., and Weckman, E. J., "Steady-State Heat Flux Measurements in Radiative and Mixed Radiative – Convective Environments," *Fire and Materials*, vol. 33, no. 7, pp. 303-321, 2009.

[16] Opila, E. J., Smialek, J. L., Robinson, R. C., Fox, D. S., Jacobson, N. S., "SiC Recession Caused by SiO_2 Scale Volatility under Combustion Conditions: II, Thermodynamics and Gaseous-Diffusion Model," *Journal of the American Ceramic Society*, vol. 82, no. 7, pp. 1826-1834, 1999.

[17] Lee, K. N., Zhu, D., and Lima, R. S., "Perspectives on Environmental Barrier Coatings (EBCs) Manufactured via Air Plasma Spray (APS) on Ceramic Matrix Composites (CMCs): A Tutorial Paper, *Journal of Thermal Spray Technology*, vol. 30, pp. 40-58, 2021.

[18] Opila, E. J., and Hann Jr., R. E., "Paralinear Oxidation of CVD SiC in Water Vapor," *Journal of the American Ceramic Society*, vol. 80, no. 1, pp. 197-205, 1997.

[19] Fox, D. S., Opila, E. J., and Hann, R. E., "Paralinear Oxidation of CVD SiC in Simulated Fuel-Rich Combustion," *Journal of the American Ceramic Society*, vol. 83, no. 7, pp. 1761-1767.

[20] Opila, E. J., Robinson, R. C., and Cuy, M. D., "High Temperature Corrosion of Silicon Carbide and Silicon Nitride in Water Vapor," *10th International Conferences on Modern Materials and Technologies* (*CIMTEC*), 2002, https://ntrs.nasa.gov.

[21] Robinson, R. C., and Smialek, J. L., "SiC Recession Caused by SiO_2 Scale Volatility under Combustion Conditions: I, Experimental Results and Empirical Model, *Journal of the American Ceramic Society*, vol. 82, no. 7, pp. 1817-1825, 1999.

[22] NASA Aeronautics Research Mission Directorate, "Commercial Supersonic Technology (CST) Project," https://www.nasa.gov/aeroresearch/programs/aavp/cst.

[23] Tacina, K., Podboy, D., and Guzman, F., "Flametube Evaluation of a Lean-Lean Combustor Concept Developed for Supersonic Cruise Aircraft," *Journal of Engineering for Gas Turbines and Power*, GTP-22-1444, 2022.

[24] Harder, B. J., Presby, M. J., Salem, J. A., Arnold, S. M., and Mital, S. K., "Environmental Barrier Coating Oxidation and Adhesion Strength," *Journal of Engineering for Gas Turbines and Power*, vol. 143, no. 3, pp. 031004-6, 2021.

[25] Lee, K. N., "$Yb_2Si_2O_7$ Environmental Barrier Coatings with Reduced Bond Coat Oxidation Rates via Chemical Modifications for Long Life," *Journal of the American Ceramic Society*, vol. 102, no. 3, pp. 1507-1521, 2018.

[26] NASA Aeronautics Research Mission Directorate, "Hybrid Thermally Efficient Core (HyTEC) Project," https://www.nasa.gov/aeroresearch/programs/hytec.

[27] Lee, K. N., Waters, D. L., Puleo, B. J., Garg, A., Jennings, W. D., Costa, G., and Sacksteder, D. E., "Development of Oxide-based High Temperature Environmental Barrier Coatings for Ceramic Matrix Composites via the Slurry Process," *Journal of the European Ceramic Society*, vol. 41, no. 2, pp. 1639-1653.